AGU PUBLICATIONS

Geophysical Research Letters

RESEARCH LETTER
10.1002/2015GL063630

Key Points:
- Seismic records used to characterize bed load transport in a low-gradient stream
- Joint analysis with hydroacoustic records and numerical bed load transport model
- Seismic monitoring useful for a broader range of rivers than previously studied

Supporting Information:
- Figures S1–S4

Correspondence to:
J. Barrière,
julien.barriere@ecgs.lu

Citation:
Barrière, J., A. Oth, R. Hostache, and A. Krein (2015), Bed load transport monitoring using seismic observations in a low-gradient rural gravel bed stream, *Geophys. Res. Lett.*, *42*, doi:10.1002/2015GL063630.

Received 25 FEB 2015
Accepted 18 MAR 2015
Accepted article online 24 MAR 2015

Bed load transport monitoring using seismic observations in a low-gradient rural gravel bed stream

Julien Barrière[1,2], Adrien Oth[2], Renaud Hostache[3], and Andreas Krein[3]

[1]National Museum of Natural History, Walferdange, Luxembourg, [2]European Center for Geodynamics and Seismology, Walferdange, Luxembourg, [3]Luxembourg Institute of Science and Technology, Environmental Research and Innovation Department, Esch-sur-Alzette, Luxembourg

Abstract The characterization of bed load transport in rivers is critical for the fundamental understanding and management of fluvial systems. Bed load monitoring based on seismological observations has recently emerged as a viable noninvasive measurement technique. However, applications of this new approach have been hitherto restricted to the case of sediment transport in steep mountain rivers. Here we further develop and evaluate the approach for a lower gradient gravel bed stream in a rural catchment using seismic observations, in situ hydroacoustic measurements of bed load motion (impact-plate-type device), and 3-D hydromorphodynamic modeling. The results of this joint analysis of seismic measurements, hydroacoustic records, and sediment transport simulations show that the seismic monitoring technique for bed load transport characterization is applicable for a broader range of river systems than previously investigated.

1. Introduction

A great portion of the sediment transported in rivers during floods originates from erosion and remobilization of bed material. Bed load causes a number of environmental problems [*Lord et al.,* 2009; *Badoux et al.,* 2014], and finding ways to adequately estimate transport rates has been a subject of significant research effort. While traditional techniques such as bed load slot samplers have been found to have strong limitations for the routine characterization of transport [*Habersack and Laronne*, 2001], vibration measurements of sediments impacting a steel plate or a pipe located on the streambed have received growing interest because this technique enables continuous measurements with high temporal resolution [*Gray et al.,* 2010; *Rickenmann et al.,* 2012]. Based on the size of the grains collected in a basket, the total mass of bed load sediments can be retrieved from impulse counting after single flood events [*Rickenmann et al.,* 2014]. The dynamics of bed load transport (e.g., start, end, and hysteresis) can also be estimated from such measurements [*Turowski et al.,* 2011; *Mao et al.,* 2014], as well as the instantaneous median grain size diameter D_{50} [*Barrière et al.,* 2015].

Over the past few years, the use of seismic sensors as a noninvasive means of measuring bed load transport has also been explored. The first such experiment was carried out by *Govi et al.* [1993], using several seismometers in the immediate vicinity of the considered test area. This easy-to-implement technique allows for a near-real time monitoring of bed load sediment transport. The potential of this so-called *fluvial seismology* to reveal the dynamics of bed load transport has already been highlighted by studies focusing on Himalayan [*Burtin et al.,* 2008, 2010], Alpine-style [*Díaz et al.,* 2014; *Burtin et al.,* 2014], Grand Canyon rivers [*Schmandt et al.,* 2013], and mountain sections of Taiwan's rivers [*Hsu et al.,* 2011; *Roth et al.,* 2014; *Chao et al.,* 2015]. Recently, *Burtin et al.* [2014] compared debris flow seismic signals in a steep Alpine catchment with impact counts from an in situ plate setup [*McArdell et al.,* 2007] located 400 m downstream from the seismic sensor. They observed a significant correlation between the seismic noise variations and the recording of transport of coarse sediments over the plate. These case studies are limited to systems where bed load transport is powerful and thus generates significant seismic signals.

In contrast to these highly energetic cases, we focus here on low-gradient streams since these have an important role for geomorphological stability of the entire river network [*Lord et al.,* 2009] and have so far received little attention. Contrary to mountain areas, the expected anthropogenic noise level in low-altitude ($<$500 m), rural catchments is generally higher because human activities are more pronounced. Furthermore, the bed load transport effect is difficult to isolate because the energy of the bed load-related seismic signal is generally weak and highly depends on grain size, channel slope, and discharge [*Tsai et al.,* 2012].

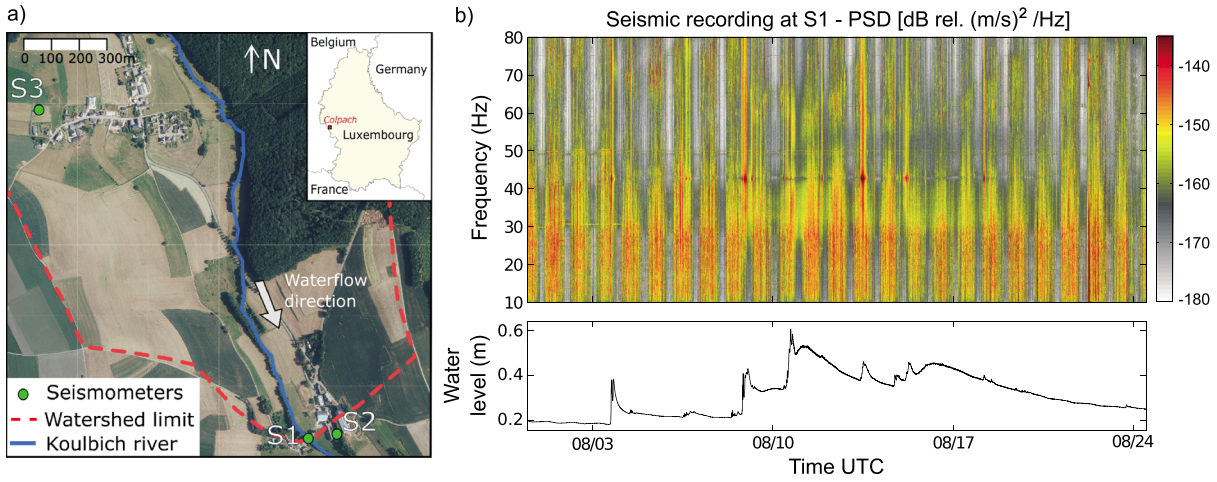

Figure 1. (a) Test site map indicating seismometer locations and (b) time-frequency map (power spectral density (PSD)) obtained using S1 during the investigated flood event and corresponding water level hydrograph.

Burtin et al. [2011] emphasized the possibility of detecting bed load transport in a mountain torrent characterized by moderate discharge (1 to 5 m^3/s) and grain sizes (D_{90} around 0.1 m). However, *Gimbert et al.* [2014] demonstrated through an elaborate physical model that the seismic recordings are largely influenced by turbulent-flow-induced noise in the case studies mentioned previously [*Burtin et al.,* 2008; *Schmandt et al.,* 2013].

In this paper, we combine seismic records, in situ impact sensor measurements, transport modeling, and hydrometeorological observations in order to investigate bed load transport phenomena in a small gravel bed river (maximum discharge $< 2.3\ m^3/s$). This allows us to compare the recorded seismic signals with in situ observations and model predictions, providing new insights into the potential and limitations of fluvial seismology for low-gradient streams.

2. Materials and Methods

2.1. Study Area and Data Acquisition

The study area is located in the upper Koulbich catchment (area of 21.5 km^2 at Colpach-Haut, Grand Duchy of Luxembourg). Colpach-Haut is a small rural town of 144 inhabitants. The Koulbich riverbed has a width ranging from 3 to 6 m, a mean slope of 0.6% in the area of interest, and is mainly composed of gravels. Samples obtained at three locations at the test site indicate that the median riverbed grain size diameter (D_{50}) ranges from 1.5 to 9.5 cm. A stream gauge at the downstream boundary of the area (~300 m elevation) recorded the water depth every 5 min, which has an annual average of a few tens of centimeters. A meteorological station located uphill (4 km away from the village) collected rainfall and wind observations.

We used three broadband seismometers (Güralp CMG-3ESPC) to record the ambient seismic field continuously (during flood events and base flow). Measurements were performed at 200 Hz sampling frequency with one sensor (S1) installed on the riverbank around 30 m upstream from the stream gauge. Two others sensors (S2 and S3) were installed at larger distances from the river (Figure 1a). Since the river-related seismic signals are likely to be of low energy and have a dominant high-frequency content [*Burtin et al.,* 2011], S1 has been placed as close as possible to the riverbed (2 m). S1 was installed on a waterproof concrete foundation and thermally shielded. To capture the seismic noise originating from the small Colpach settlement and especially the nearby farm, S2 was placed next to the farm 100 m away from S1. S3 was installed at more than 1 km distance from S1 in a low-noise environment (buried municipal water tank). As a test case we selected the August 2014 flood event (Figure 1b) with water depths ranging from 0.18 to 0.6 m corresponding to flow rates between 3.3 $10^{-2}\ m^3/s$ and 2.26 m^3/s.

The hydroacoustic system was located on the streambed near seismometer S1. It is composed of a piezoelectric hydrophone acting as a "sediment vibration sensor" in contact with a squared steel plate of 50 cm width. In addition, a sediment trap was buried downstream of the plate to collect the solid material transported during

flood events. The collected material was sifted and weighted after every major flood event. An overview of the installed equipment is shown in the supporting information (Figure S1). For the considered flood event, hydroacoustic data were available until 13 August only due to data storage limitations. Given that the plate is only located about 20 m downstream from seismometer S1, the corresponding impact records represent a key data set constraining the seismic observations as well as evaluating the bed load transport model presented hereafter.

2.2. Seismic Data Processing

We computed time-frequency maps of power spectral density (PSD) with 75% overlapping time windows of 2.44 min (2^{15} samples) duration following a processing approach developed for ambient noise analysis [*McNamara and Buland,* 2004]. According to the expected high-frequency content of very local fluvial processes, the time-frequency PSD obtained at S1 is centered on frequencies between 10 and 80 Hz (Figure 1b). The rural environment with farming activities as well as the nearby village roads necessarily leads to anthropogenic disturbances on the recorded seismograms that are pronounced during the day with typical diurnal cycles. The highest ambient noise levels cover a wide dominant frequency band between 10 and 50 Hz, and the extraction of potential PSD variations due to hydrodynamic effects, therefore, necessitates postprocessing these data. Since the expected bed load transport signals are of low energy, we selected the tenth percentile (P10) from the original time-frequency map for each frequency subband and 24 h interval overlapped by 1 h. This procedure eliminates to a large extent the effects of large-amplitude transients mostly related to anthropogenic activities. A 24 h interval has been considered to ensure the robustness of the statistical calculation between successive days while the 1 h overlap is used to smooth the final P10 time-frequency map. The resulting P10 map, however, still exhibits a diurnal cycle potentially hampering a straightforward interpretation of P10 values between successive days. As a result, the seismic response to river processes could be masked or exaggerated because flood events generally last for several days. We, therefore, applied an additional processing step on the raw PSD data before calculating P10 as illustrated in Figure S2. For each frequency, the raw PSD map is filtered (zero-phase Butterworth high-pass filtering) to remove the diurnal cycle, with the sampling period set to the time window of PSD calculation (i.e., 2.44 min) and the cutoff period set to 1 h. The filtered PSD map allows the night and day ambient noise levels to be scaled to the same constant base value (the mean PSD over the entire period) rather than an irregular daily sinusoid. As a result, the final estimation of the tenth percentile (P10) is less affected by daily patterns. The low cutoff period (i.e., 1 h) thus mitigates the main diurnal cyclic components of cultural noise as well as any additional long-lasting sinusoidal variations of several hours duration.

2.3. Hydroacoustic Impact-Plate Data Processing

Using the same in situ apparatus as in this study, *Barrière et al.* [2015] demonstrated that qualitative as well as essential quantitative information about bed load transport can be derived at high temporal resolution (minutes). The first property easily extracted from the raw data, which are recorded at 96 kHz sampling rate, is the number of counts over a minimum noise floor threshold, which describes qualitatively the bed load transport rate as shown for instance by *Mao et al.* [2014]. The instantaneous median grain diameter D_{50} can also be estimated from impact amplitude and frequency characteristics using a laboratory-derived calibration curve (for D_{50} greater than 1 mm, see *Barrière et al.* [2015] for more details). This derived parameter is associated with a mean D_{50} of transported material over a 5 min interval. The impact-plate setup thus provides localized information on the order of magnitude of transport rates and the grain size distribution of bed load material moving over the plate.

2.4. Three-Dimensional Hydromorphodynamic Model

We used a hydromorphodynamic model to simulate bed load transport during the selected August 2014 flood event based on the Telemac hydroinformatic system, release 6.2 [*Hervouet and Bates*, 2000]. This system dynamically couples a three-dimensional hydrodynamic model (Telemac-3-D) and a one-dimensional sediment transport/morphodynamic model (Sysiphe) with an identical time step. Telemac-3-D solves the Navier-Stokes equations while Sysiphe simulates the bed evolution using the Exner equation and proposes many established semiempirical equations for solid transport. In addition, it offers the ability to decompose the transport processes into bed load and suspended load (see *Hostache et al.* [2014] for more details). The terrain and riverbed are represented by an unstructured triangular mesh with refinement in the riverbed

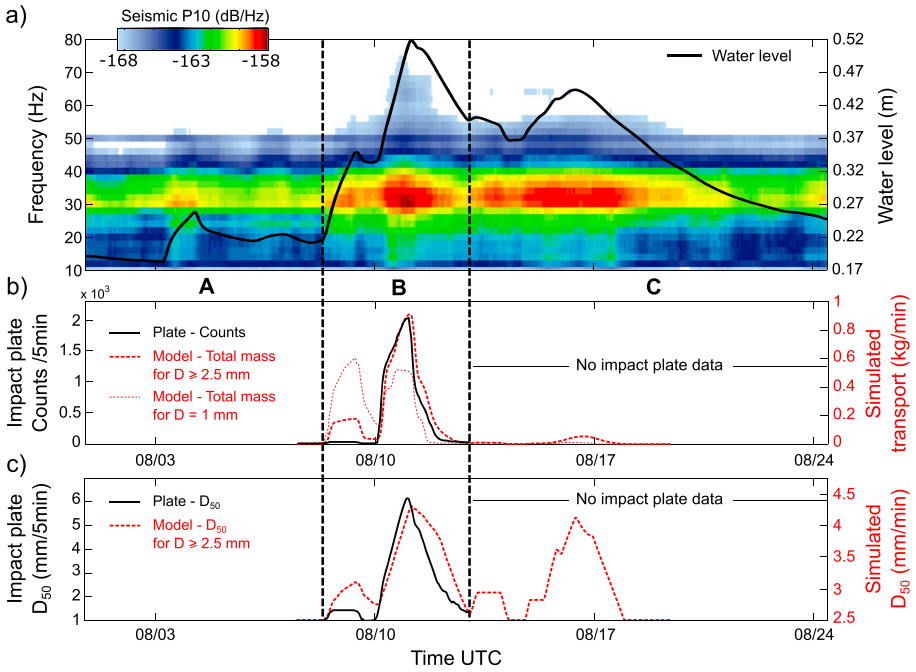

Figure 2. (a) Water discharge and P10 extracted from the PSD map. (b) Impact-plate data versus bed load transport model: Simulated transported bed load mass (red dashed lines) and counts (black line) above a minimum "noise floor" threshold and (c) simulated (red dashed line) and estimated D_{50} (black line) using impact-plate data and the method developed in *Barrière et al.* [2015]. For a reliable comparison, all data displayed in this figure correspond to 24 h averaged values according to the seismic processing.

area (the distance between two nodes ranges from 0.3 to 2 m in the riverbed). The various bed load transport equations programmed in Sysiphe ensure that the model is adaptable to various river types. We chose the Einstein-Brown equation designed for large sediment grain size as the bed load transport equation. Trial and error tests over all bed load transport equations implemented in Sysiphe showed that only this equation was able to provide realistic results in terms of erosion and deposition rates. The boundary conditions of the model were defined from an upstream observed flow discharge hydrograph and a downstream observed water level hydrograph. The bed load transport rate boundary conditions are free.

The riverbed material grading curve was spatially distributed based on three bed material samplings. Seven classes of sediment grain size were defined in the model corresponding to representative bed material diameters $D = [1, 2.5, 5, 7.5, 10, 25, 50]$ mm. The model simulates erosion, deposition, and bed load transport rates for each sediment class independently. From a hydrodynamic point of view, the model was evaluated against an additional water depth hydrograph observed at the hydroacoustic plate location. The corresponding Nash Sutcliffe Efficiency [*Nash and Sutcliffe*, 1970] value obtained is close to one, indicating a good reliability of the model.

After the flood event (1 September 2014), around 80 kg of sediment was retrieved in the basket sampler, which was filled to its maximum capacity. The D_{50} of the collected material was around 3 mm and was in good agreement with the modeled value; the D_{50} of the deposited material simulated by the model in a "virtual basket sampler" was 2 mm. Moreover, based on the time evolution of simulated transported mass, the model suggests that the basket was probably already filled (i.e., 80 kg) at the beginning of the main peak flow (9 August, Figure 1c). All simulated bed load data shown hereafter have been extracted from the mesh node corresponding to the impact-plate location.

3. The Stream's Seismic Signature in a Multimethod Framework

We focus here on P10 changes at station S1 with time and frequency and discuss how these changes relate to the impact-plate data and bed load transport modeling results (Figure 2). Note that only station S1 directly located on the riverbank exhibits clear P10 variations over the course of the flood event, while P10 estimates

at S2 and S3 are free of any particular signature (Figure S3). The time series in Figure 2 can be divided into three main phases (A to C) related to the dynamics of water flow and bed load transport: phase A corresponds to low water discharge, phase B to the main flow peak with steep rising limb, and phase C to a secondary flow peak with smoother rising and falling limbs.

3.1. P10 Power Spectral Density Variations in Time and Frequency

During phase A, the P10 time-frequency map exhibits a significant peak in the range 30–35 Hz during the small water level peak on 4 August (Figure 2a). No impacts were counted with the hydroacoustic setup, and no bed load transport was predicted by the model during the same base flow period (Figure 2b). Water depth increases during phase B, and the P10 values show a correlated broadband increase of P10 levels in the range 10–70 Hz during the two successive discharge peaks with pronounced maxima in the 30–40 Hz band. Furthermore, note that the maximum P10 values are also very well correlated in time with the maximum 24 h averaged counts from plate measurements, which follows a similar trend as the bed load mass predicted by the model for $D \geq 2.5$ mm (Figure 2b). This correlation is not observed for the model curve corresponding to $D = 1$ mm. This discrepancy can be explained by the fact that both seismic and plate measurements are less sensitive to the finest grain size sediments transported by saltation as well as suspension mode. We also compare the mean D_{50} estimated with the plate setup following *Barrière et al.* [2015] and the simulated bed load D_{50} (Figure 2c). As the smallest model grain class (1 mm) is a limiting case for the impact plate, it is not taken into account in this calculation. Although the D_{50} time series predicted by the model has a slightly limited range compared to the one derived from the impact-plate record, both simulated and estimated D_{50} from impact-plate measurements exhibit near-simultaneous increases, similar temporal evolution, and the same order of magnitude. The overall P10 signature of phase B, therefore, potentially results from additive hydrodynamic and bed load transport processes since significant gravel material is transported during this event (Figures 2b and 2c). Finally, the P10 signature during phase C (no impact-plate data available) can be associated with the fluctuations of water discharge as well as moderate bed load transport, according to the modeling results (Figures 2b and 2c).

Identical P10 temporal variations are also obtained for the horizontal components but shifted by about 10 dB toward higher magnitude values and by about 10 Hz to lower frequency content (dominating frequency band around 20 Hz). No clear relationships between prevailing moderate meteorological conditions (wind and rain) and P10 attributes were observed (Figure S4). P10 variations are similar in both horizontal components (NS and EW), which may be related to the NW-SE stream direction in the area of interest and horizontal forces dominated by water flow processes (i.e., shear stress mostly parallel to the riverbed). If bed load transport is idealized as a force normal to the riverbed [*Tsai et al.,* 2012], which is associated to the saltation mode in this case, the preferential generation of Rayleigh waves could explain part of the P10 changes in the vertical direction. However, the various bed load transport modes, especially rolling and sliding, are probably significant factors able to generate additional horizontally polarized surface waves (Love waves). As already pointed out by *Schmandt et al.* [2013], this may explain high power levels on the horizontal spectra as also obtained in their study (Hance Rapids, Colorado River).

Gimbert et al. [2014] demonstrated from a theoretical approach that frictional forces due to turbulent flow reacting to bed roughness in gravel bed rivers are responsible to a large extent for the seismic noise recorded close to the Trisuli river in Nepal [*Burtin et al.,* 2008] and that these explain spectral peaks at low frequency (6–7 Hz) observed at Hance Rapids in the Colorado river [*Schmandt et al.,* 2013]. Although they only focus on the vertical component, *Gimbert et al.* [2014] discuss that turbulent flow noise sources generate a combination of Rayleigh and Love waves that are recorded by the vertical and horizontal components of seismic stations in a comparable high-frequency range (1–100 Hz). Hence, our observations at the Koulbich River are likely due to a combination of dominating fluctuating forces controlled by water flow on the rough riverbed and bed load-induced noise during periods of high water discharge. *Gimbert et al.* [2014] pointed out that turbulent flow-induced noise occurs at lower frequencies than bed load-generated seismic noise. This might explain the fact that the horizontal components exhibit stronger amplitude levels at lower frequency in comparison to the vertical one (Figure S4) because they are more sensitive to water flow processes than bed load transport. However, these distinct frequency regimes are overlapping, leading to difficulties in separating both signatures as observed in our results as well as in the aforementioned studies [*Burtin et al.,* 2008; *Schmandt et al.,* 2013].

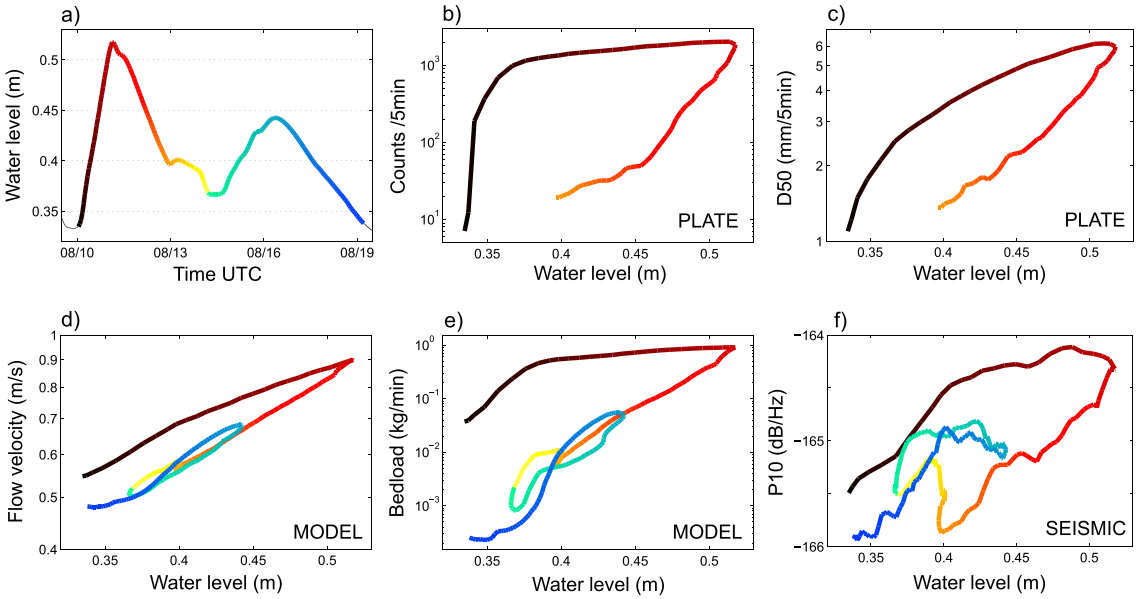

Figure 3. (a) Selected portion of the flood event constituted by two flow peaks between 10 and 19 August. Variations of (b) impact-plate counts, (c) estimated mean D_{50}, (d) flow velocity, (e) simulated bed load mass for $D \geq 2.5$ mm, and (f) P10 averaged over the entire frequency band [10–80] Hz, as a function of water level. Color variations in Figure 3a correspond to successive time steps displayed on each panels in Figures 3b–3f. For a reliable comparison, all data displayed in this figure correspond to 24 h averaged values according to the seismic processing. Note that *y* axes for Figures 3b–3f are expressed in log scale and no impact plate data are available for the second flood event (after 13 August).

3.2. Evidence of Bed Load Transport Effect

Well-developed seismic PSD hysteresis behavior as a function of water level has been interpreted as a direct result of bed load transport in recent studies [*Burtin et al.,* 2008; *Hsu et al.,* 2011; *Schmandt et al.,* 2013; *Díaz et al.,* 2014; *Roth et al.,* 2014; *Chao et al.,* 2015] because sediment motion during flood events is often characterized by different transport rates during the rising and falling limbs [*Mao*, 2012]. The reliability of this interpretation has been difficult to prove due to partial or total lack of in situ information in these previous studies, which largely focused on mountain systems. Our multimethod approach allows new insights on this issue through comparison of collocated impact-plate and seismic measurements as well as transport modeling results.

Figure 3 depicts, for the successive events between 10 and 19 August (Figure 3a), the variations of impact-plate counts, transported D_{50}, simulated flow velocity and bed load transport rate (for $D \geq 2.5$ mm), and seismic P10 estimates averaged over the entire frequency band [10–80] Hz as a function of water level (Figures 3b–3f, respectively). A similar clockwise hysteresis is obtained for both simulated bed load transport rate and hydroacoustic measurements, as well as for the P10 values, which is characterized by a mean width of around 1 dB. However, this hysteresis by itself is not necessarily a direct evidence of bed load effect, as flow velocity can exhibit hysteretic behavior as well and, as mentioned previously, turbulence can be responsible for strong PSD changes [*Gimbert et al.,* 2014]. From their model, *Gimbert et al.* [2014] proposed that the PSD of the seismic signal due to the turbulent flow can be related to the shear velocity and, consequently, the flow velocity, through a power law. According to this relationship, the PSD should thus change linearly with the logarithm of the flow velocity. To identify whether the recorded seismic signal is mainly a consequence of the turbulent flow or the bed load transport, we examined the flow velocity, as simulated by the model, at the impact-plate location (Figure 3d). In Figure 3d, the flow velocity plotted against the water level exhibits a rather limited hysteresis behavior that alone cannot explain the hysteresis of the P10 data in Figure 3f. This result is in agreement with the study of *Hsu et al.* [2011], as they argued that the flow turbulence alone cannot explain the large development of the hysteresis of PSD with respect to water depth. Consequently, the P10 changes recorded during the first peak are mainly the result of bed load transport. During the second peak, no significant transport is simulated by the model and the P10 increase is limited as well. No evident hysteresis behavior is visible for the second peak on the simulated flow velocity and bed load curves. Furthermore, note

that the reasonably pronounced bending for each hysteresis curve occurs at water level between 0.35 and 0.4 m during the first rising limb and the strong similarity in shape between the seismic, the transported D_{50}, and the simulated bed load mass hystereses. This implies that the observed seismic signature is directly related to the amount of transported sediment and its grain size distribution. Thus, a coherent seismic response to bed load transport seems detectable when a given transport threshold of coarse material is exceeded. In our case, the P10 level exceeds −165 dB/Hz during the first rising limb due to the significant motion of coarser sediments as predicted by the model (until 0.9 kg/min at the plate location) and observed in the hydroacoustic measurements (more than 10^3 counts/5 min with $D_{50} > 3$ mm).

In bed load transport equations, the discharge threshold needed to activate bed load transport is an essential parameter [*Ferguson*, 1994; *Lenzi et al.,* 2006; *Lamb et al.,* 2008]. While *Turowski et al.* [2011] proposed using impact-plate measurements to detect the inception of bed load motion in four gravel bed mountain streams, an appropriate seismic sensor located on the riverbank seems to be sensitive enough to the start and end of gravel motion even in a small stream with low discharge (maximum discharge $< 2.3\ m^3/s$). As discussed by *Gimbert et al.* [2014], the strength of the hysteresis depends on the contribution of bed load transport to the overall ambient noise that is dominated by turbulent flow-induced processes. Considering the higher frequency regime of bed load-induced noise, a more pronounced hysteresis should occur at higher frequency. This frequency dependence has not been clearly detected here due to the rather weak P10 variations, and one can potentially expect such a frequency-dependent hysteresis in the case of coarser sediment motion and higher transport rates.

4. Conclusions

We evaluated for the first time the potential of fluvial seismology for bed load transport monitoring in a rural gravel bed stream, characterized by low gradient (around 0.6%), small flow rate ($<2.3\ m^3/s$) and small D_{50} transported (around 5 mm on average). The dominant anthropogenic noise in the area of investigation greatly increased the complexity of the seismic analysis but was successfully eliminated in order to extract the river's imprint on the ambient seismic field. In addition, it must be mentioned that station S1 is located in the near field with respect to the source zone of the seismic signals of interest for the overall frequency band of analysis. This represents some direct limitations for the use of river-induced seismic noise models [*Tsai et al.,* 2012; *Gimbert et al.,* 2014], but we showed, in accordance with additional in situ and modeling information, that the seismic data recorded in close proximity of the stream contain evidence of bed load transport, especially in the form of hysteresis behavior. These results underline the potential of noninvasive seismic measurements to estimate the triggering of bed load transport for a wide range of river systems and grain sizes (i.e., diameter exceeding few millimeters) and consequently to better constrain models and reduce prediction uncertainties.

Acknowledgments

This study was supported by the National Research Fund, Luxembourg (BEDLOAD C11/SR/1158445). Field assistance was provided by J.F. Iffly. We thank V. Tsai and L. Hsu for their constructive reviews and R.L. Thompson for manuscript proof reading. Seismic, hydroacoustic, and hydrometeorological data were recorded and collected by the European Center for Geodynamics and Seismology (www.ecgs.lu) and the Luxembourg Institute of Science and Technology (www.list.lu). Raw data (6.16 GB seismic files in mSEED format, 32 GB hydroacoustic files in WAV format), preprocessed (4.42 GB: PSD maps, instantaneous hydroacoustic counts and mean D_{50}, hydromorphodynamic model, water level, and meteorological data) and final 24 h averaged data (360 KB) in ASCII format may be retrieved at ftp://bedload@ftp.ecgs.lu (password on demand, contact julien.barriere@ecgs.lu). Processing scripts written in the MATLAB® R2013a environment can be also obtained upon request.

The Editor thanks Leslie Hsu for her assistance in evaluating this paper.

References

Badoux, A., N. Andres, and J. M. Turowski (2014), Damage costs due to bedload transport processes in Switzerland, *Nat. Hazards Earth Syst. Sci.*, *14*, 279–294, doi:10.5194/nhess-14-279-2014.

Barrière, J., A. Krein, A. Oth, and R. Schenkluhn (2015), An advanced signal processing technique for deriving grain size information of bedload transport from impact plate vibration measurements, *Earth Surf. Processes Landforms*, doi:10.1002/esp.3693.

Burtin, A., L. Bollinger, J. Vergne, R. Cattin, and J. L. Nabelek (2008), Spectral analysis of seismic noise induced by rivers: A new tool to monitor spatiotemporal changes in stream hydrodynamics, *J. Geophys. Res.*, *113*, B05301, doi:10.1029/2007JB005034.

Burtin, A., R. Cattin, L. Bollinger, J. Vergne, P. Steer, A. Robert, N. Findling, and C. Tiberi (2011), Towards the hydrologic and bed load monitoring from high-frequency seismic noise in a braided river: The "torrent de St Pierre", French Alps, *J. Hydrol.*, *408*(1–2), 43–53, doi:10.1016/j.jhydrol.2011.07.014.

Burtin, A., N. Hovius, B. W. McArdell, J. M. Turowski, and J. Vergne (2014), Seismic constraints on dynamic links between geomorphic processes and routing of sediment in a steep mountain catchment, *Earth Surf. Dyn.*, *2*, 21–33, doi:10.5194/esurf-2-21-2014.

Chao, W.-A., Y.-M. Wu, L. Zhao, V. C. Tsai, and C.-H. Chen (2015), Seismologically determined bedload flux during the typhoon season, *Sci. Rep.*, *5*, doi:10.1038/srep08261.

Díaz, J., M. Ruíz, L. Crescentini, A. Amoruso, and J. Gallart (2014), Seismic monitoring of an Alpine mountain river, *J. Geophys. Res. Solid Earth*, *119*, 3276–3289, doi:10.1002/2014JB010955.

Ferguson, R. I. (1994), Critical discharge for entrainment of poorly sorted gravel, *Earth Surf. Processes Landforms*, *19*, 179–186, doi:10.1002/esp.3290190208.

Gimbert, F., V. C. Tsai, and M. P. Lamb (2014), A physical model for seismic noise generation by turbulent flow in rivers, *J. Geophys. Res. Earth Surf.*, *119*, 2209–2238, doi:10.1002/2014JF003201.

Govi, M., F. Maraga, and F. Moia (1993), Seismic detectors for continuous bed load monitoring in a gravel stream, *Hydrol. Sci. J.*, *38*(2), 123–132.

Gray, J. R., J. B. Laronne, and J. D. G. Marr (2010), Bedload-surrogate monitoring technologies, U.S. Geological Survey Scientific Investigations Report 2010–5091.

Habersack, H. M., and J. B. Laronne (2001), Bedload texture in an alpine gravel bed river, *Water Resour. Res.*, *37*(12), 3359–3370, doi:10.1029/2001WR000260.

Hervouet, J.-M., and P. Bates (2000), The TELEMAC modelling system—Special issue, *Hydrol. Processes*, *14*, 2207–2208.

Hostache, R., C. Hissler, P. Matgen, C. Guignard, and P. Bates (2014), Modelling suspended-sediment propagation and related heavy metal contamination in floodplains: A parameter sensitivity analysis, *Hydrol. Earth Syst. Sci.*, *18*, 3539–3551, doi:10.5194/hess-18-3539-2014.

Hsu, L., N. J. Finnegan, and E. E. Brodsky (2011), A seismic signature of river bed-load transport during storm events, *Geophys. Res. Lett.*, *38*, L13407, doi:10.1029/2011GL047759.

Lamb, M. P., W. E. Dietrich, and J. G. Venditti (2008), Is the critical Shields stress for incipient sediment motion dependent on channel-bed slope?, *J. Geophys. Res.*, *113*, F02008, doi:10.1029/2007JF000831.

Lenzi, M. A., L. Mao, and F. Comiti (2006), When does bedload transport begin in steep boulder-bed streams?, *Hydrol. Processes*, *20*, 3517–3533, doi:10.1002/hyp.6168.

Lord, M. L., D. Germanoski, and N. E. Allmendinger (2009), Fluvial geomorphology: Monitoring stream systems in response to a changing environment, in *Geological Monitoring, Boulder*, edited by R. Young and L. Norby, pp. 69–103, Geol. Soc. Am., Boulder, Colo.

Mao, L. (2012), The effect of hydrographs on bed load transport and bed sediment spatial arrangement, *J. Geophys. Res.*, *117*, F03024, doi:10.1029/2012JF002428.

Mao, L., A. Dell'Agnese, C. Huincache, D. Penna, M. Engel, G. Niedrist, and F. Comiti (2014), Bedload hysteresis in a glacier-fed mountain river, *Earth Surf. Processes Landforms*, doi:10.1002/esp.3563.

McArdell, B. W., P. Bartelt, and J. Kowalski (2007), Field observations of basal forces and fluid pore pressure in a debris flow, *Geophys. Res. Lett.*, *34*, L07406, doi:10.1029/2006GL029183.

McNamara, D. E., and R. P. Buland (2004), Ambient noise levels in the continental United States, *Bull. Seismol. Soc. Am.*, *94*(4), 1517–1527.

Nash, J. E., and J. V. Sutcliffe (1970), River flow forecasting through conceptual models. Part I: A discussion of principles, *J. Hydrol.*, *10*, 282–290.

Rickenmann, D., J. M. Turowski, B. Fritschi, A. Klaiber, and A. Ludwig (2012), Bedload transport measurements at the Erlenbach stream with geophones and automated basket samplers, *Earth Surf. Processes Landforms*, *37*, 1000–1011, doi:10.1002/esp.3225.

Rickenmann, D., et al. (2014), Bedload transport measurements with impact-plate geophones: Comparison of sensor calibration in different gravel-bed streams, *Earth Surf. Processes Landforms*, *39*, 928–942, doi:10.1002/esp.3499.

Roth, D. L., N. J. Finnegan, E. E. Brodsky, K. L. Cook, C. P. Stark, and H. W. Wang (2014), Migration of a coarse fluvial sediment pulse detected by hysteresis in bedload generated seismic waves, *Earth Planet. Sci. Lett.*, *404*, 144–153, doi:10.1016/j.epsl.2014.07.019.

Schmandt, B., R. C. Aster, D. Scherler, V. C. Tsai, and K. Karlstrom (2013), Multiple fluvial processes detected by riverside seismic and infrasound monitoring of a controlled flood in the Grand Canyon, *Geophys. Res. Lett.*, *40*, 4858–4863, doi:10.1002/grl.50953.

Tsai, V. C., B. Minchew, M. P. Lamb, and J.-P. Ampuero (2012), A physical model for seismic noise generation from sediment transport in rivers, *Geophys. Res. Lett.*, *39*, L02404, doi:10.1029/2011GL050255.

Turowski, J. M., A. Badoux, and D. Rickenmann (2011), Start and end of bedload transport in gravel-bed streams, *Geophys. Res. Lett.*, *38*, L04401, doi:10.1029/2010GL046558.